Nonlinear response of summer temperature to Holocene insolation forcing in Alaska

Benjamin F. Clegg[a,b], Ryan Kelly[b], Gina H. Clarke[b,1], Ian R. Walker[c], and Feng Sheng Hu[a,b,d,2]

[a]Program in Ecology, Evolution, and Conservation Biology, [b]Department of Plant Biology, and [d]Department of Geology, University of Illinois, Urbana, IL 61801; and [c]Biology and Earth and Environmental Sciences, University of British Columbia Okanagan, Kelowna, BC, Canada V1V 1V7

Edited by Mark H. Thiemens, University of California San Diego, La Jolla, CA, and approved October 21, 2011 (received for review July 8, 2011)

Regional climate responses to large-scale forcings, such as precessional changes in solar irradiation and increases in anthropogenic greenhouse gases, may be nonlinear as a result of complex interactions among earth system components. Such nonlinear behaviors constitute a major source of climate "surprises" with important socioeconomic and ecological implications. Paleorecords are key for elucidating patterns and mechanisms of nonlinear responses to radiative forcing, but their utility has been greatly limited by the paucity of quantitative temperature reconstructions. Here we present Holocene July temperature reconstructions on the basis of midge analysis of sediment cores from three Alaskan lakes. Results show that summer temperatures during 10,000–5,500 calibrated years (cal) B.P. were generally lower than modern and that peak summer temperatures around 5,000 were followed by a decreasing trend toward the present. These patterns stand in stark contrast with the trend of precessional insolation, which decreased by ∼10% from 10,000 y ago to the present. Cool summers before 5,500 cal B.P. coincided with extensive summer ice cover in the western Arctic Ocean, persistence of a positive phase of the Arctic Oscillation, predominantly La Niña-like conditions, and variation in the position of the Alaskan treeline. These results illustrate nonlinear responses of summer temperatures to Holocene insolation radiative forcing in the Alaskan sub-Arctic, possibly because of state changes in the Arctic Oscillation and El Niño-Southern Oscillation and associated land–atmosphere–ocean feedbacks.

Chironomidae | paleotemperature | climate change | high latitudes | land–ocean–atmosphere interaction

Although radiative forcing by greenhouse gases is spatially uniform, temperature trajectories have displayed high variability both spatially and temporally during the 20th and 21st centuries. Understanding the patterns and causes of this variability is paramount to anticipating the impacts of climate change at local to regional scales. Among the major contributing factors is nonlinearity in regional temperature responses to large-scale climate forcings. Such nonlinearity may result from land–ocean feedbacks to atmospheric warming and atmosphere–ocean teleconnections associated with climate modes such as the Arctic Oscillation/North Atlantic Oscillation (AO/NAO) (1). For example, rising global mean temperatures are projected to increase prevalence of the AO/NAO positive phase by the end of this century. This change could accentuate the contrast of warming over Eurasia and interior Canada with cooling over northeastern Canada.

Paleorecords can help elucidate mechanisms leading to nonlinear and spatially heterogeneous responses of temperature to radiative forcing. During the Holocene, high-latitude insolation varied markedly with the precessional cycle; for example, July short-wave radiation declined by ∼50 W m^{-2} at 65° N latitude throughout the Holocene (2). Paleoclimate data and model simulations have demonstrated the dominant effect of decreasing insolation on the Holocene temperature trends of many Arctic regions (3). A recent synthesis of paleoclimate reconstructions from the western Arctic also found broad consistency in the spatial patterns of the Holocene thermal maximum and 20th century warming, attributed to possible effects of the AO during both periods (4). Some outstanding exceptions to this consistency do exist. In particular, Alaska is thought to have experienced a thermal maximum during the early Holocene, in contrast to cooling expected from a possible positive phase of AO. The existence of *Populus* woodland as inferred from some Alaskan pollen records is often cited as evidence of an early-postglacial thermal maximum (4). However, this interpretation remains controversial (5), and paleoecologists have struggled with the conflict that tundra prevailed on today's forested areas during the early Holocene when the regional climate was putatively warmer than today. Resolving these issues requires Holocene summer-temperature reconstructions, but such records are scarce despite several decades of paleoclimate research (6, 7).

Transfer functions relating midge assemblages to mean July air temperature (T_{July}) are considered one of the most reliable means for past temperature reconstruction. We analyzed sediment cores from three Alaskan lakes for midge assemblages. Results provide quantitative estimates of temperature change from the high-latitude North Pacific sector. This study offers evidence for nonlinear responses to precessional insolation forcing at the regional scale, dispelling the long-standing assumption that the early-to-middle Holocene was warmer than later in sub-Arctic Alaska. Our data also suggest that land–atmosphere–ocean feedback processes played a key role in determining Holocene temperature trajectories.

Study Sites

Hudson Lake (61° 54′N, 145° 40′W, 657 m above sea level) is located on the southern edge of the Copper River Basin, south-central Alaska (Fig. 1). The lake is an open basin with a small inlet and a small outlet, a surface area of 256.2 ha, and a maximal water depth of 14.0 m. It is situated on a plateau in the foothills of the Chugach Mountains. The lake sits on silty sediments deposited by proglacial Lake Atna, which covered most of the Copper River Basin during the Pleistocene. Today Hudson Lake is surrounded by closed boreal forest with tall *Picea glauca* stands on the steeper slopes and *Picea mariana* stands on poorly drained areas to the southwest. Modern climate is continental, with an average July temperature of 14.1 °C at the Gulkana weather station, ∼40 km north-northwest of the lake. A small camp associated with a correctional facility lies on a ridge overlooking the lake on the eastern shore.

Screaming Lynx Lake (66° 04′N, 145° 24′W, 223 m above sea level) is situated within the Yukon Flats, east-central Alaska.

Author contributions: B.F.C. and F.S.H. designed research; B.F.C. and G.H.C. performed research; R.K. contributed new reagents/analytic tools; B.F.C. and I.R.W. analyzed data; and B.F.C. and F.S.H. wrote the paper.

The authors declare no conflict of interest.

This article is a PNAS Direct Submission.

[1]Present address: Environmental Change Research Centre, University College London, Pearson Bldg., Gower St., London WC1E 6BT, UK.

[2]To whom correspondence should be addressed. E-mail: fshu@life.illinois.edu.

This article contains supporting information online at www.pnas.org/lookup/suppl/doi:10.1073/pnas.1110913108/-/DCSupplemental.

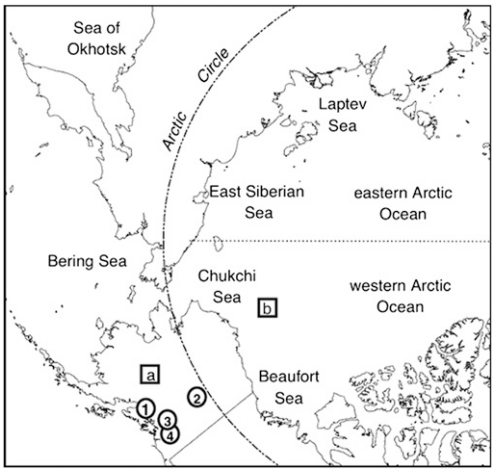

Fig. 1. Map of sites and locations mentioned in text. Numbered circles correspond to quantitative temperature reconstructions included in our temperature composite (Fig. 3): 1, Rainbow Lake; 2, Screaming Lynx Lake; 3, Hudson Lake; 4, Moose Lake (7). Lettered squares correspond to midge-independent climate records compared with our midge-temperature composite (Fig. 4): a, Farewell Lake (5); b, dinoflagellate-inferred sea-ice record in the Chukchi Sea (8).

The lake is a groundwater-fed, topographically closed basin with a surface area of 3.5 ha and a maximal depth of 7.4 m. Early-successional deciduous forests resulting from a fire in historical times dominate the watershed vegetation today. Remaining patches of prefire vegetation indicate that a closed forest dominated by *P. glauca* and *Betula neoalaskana* surrounded the lake. Tall *Salix* shrubs form a dense understory near the lake margin. Modern climate is continental, and July temperatures and temperature seasonality in this area are among the highest in Alaska. Mean July temperature is 16.8 °C at the Fort Yukon weather station, located ∼55 km north of the lake.

Rainbow Lake (60° 43′N, 150° 48′W, 63 m above sea level) is located in the northwestern lowlands of the Kenai Peninsula, southern Alaska. It is situated between the Kenai Mountains and the Alaskan Range on till of a late-Pleistocene ground moraine. The lake is fed by shallow groundwater and overflows from a small outlet on its western shore. It has a surface area of 67.1 ha and a maximal water depth of 4.8 m. Today the lake is surrounded by closed boreal forest dominated by *P. glauca*, *Populus tremuloides*, and *Betula kenaica*. Modern climate is transitional maritime/continental, with an average July temperature of 12.6 °C at the Kenai Airport weather station, ∼29 km southwest of the lake. A road passes the lake within 40 m, and a campground with boat access is located on the western shore of the lake.

Results and Discussion

Reliability of Midge-Based Temperature Reconstruction. Although midge temperature transfer functions have relatively large error envelopes (9–11), they have proven to provide reliable T_{July} estimates when tested against instrumental and tree-ring temperature records in Alaska and elsewhere (e.g., refs. 7, 12). The large error envelopes can be at least partially attributed to the wide range of limnological and watershed characteristics of the lakes from which surface (modern) sediments were collected for midge analysis to develop temperature transfer functions. These characteristics should have remained comparatively constant through time at any given site where midge assemblages are used to infer Holocene T_{July} shifts (7). A number of recent studies in various regions (e.g., refs. 7, 12, 13), including Alaska, have successfully applied midge analysis to infer Holocene T_{July} variation.

At Hudson, Rainbow, and Screaming Lynx lakes, midge assemblages are dominated by littoral chironomid genera, as expected for these relatively shallow lakes. The assemblages vary predictably with the modern temperature gradient across these sites and the bathometric settings. Cold-stenotherm taxa (e.g., *Sergentia* and *Micropsectra*) typical of cold, high-Arctic lakes are most abundant at Hudson Lake (Fig. S1), reflecting the colder temperature at this lake than at the other two sites. The greater water depth at Hudson Lake may also promote thermal stratification and allow these taxa to persist in cool, profundal waters despite the boreal setting of the lake. For comparison, midge assemblages at Screaming Lynx Lake are skewed toward taxa with warm temperature optima, including the thermophilic taxa *Chaoborus* and *Labrundinia* (Fig. S2). These among-site differences in midge assemblages are captured by estimated T_{July} values from the surface (modern) sediments, which increase from Hudson Lake to Rainbow Lake (Fig. S3) to Screaming Lynx Lake. These T_{July} estimates along with that from Moose Lake in Alaska (7) compare favorably with instrumental temperature data from the nearest weather stations to each lake, after correcting for elevational differences between lakes and weather stations using a dry adiabatic rate of 9.8 °C/km (r = 0.995, $P < 0.01$, n = 4).

The reliability of midge-based T_{July} estimates is also evidenced by the broad consistency of decadal-resolution temperature reconstructions between midge and tree-ring temperature records within the same region. Within the chronological constraints of the lake-sediment records, a local T_{July} minimum around 200 calibrated years (cal) B.P. at Hudson Lake also occurred at a nearby midge record from Moose Lake (7). This minimum during the Little Ice Age roughly coincides with minimal temperature estimates on the basis of tree-ring records from the adjacent Wrangell Mountains (Fig. 2 *A* and *B*) (14, 15). These midge and tree-ring records all display temperature increases that began around 150 cal B.P. Verifying T_{July} estimates from Screaming Lynx Lake is more difficult, because no tree-ring record of

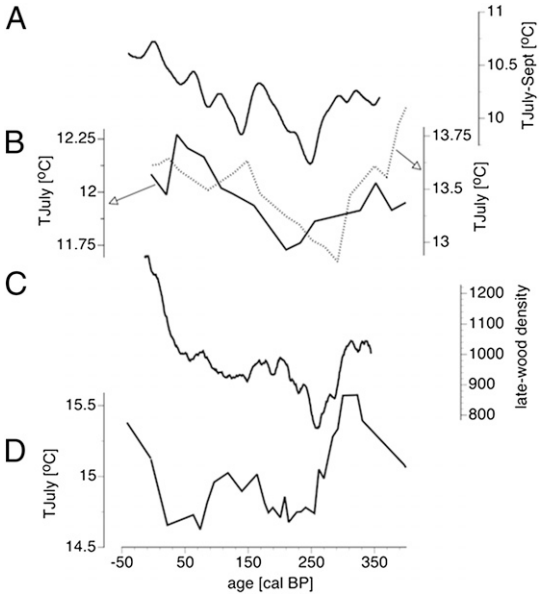

Fig. 2. Comparison of (*A*) tree-ring–inferred summer temperature in the Wrangell Mountains (50 y running mean) (14) with (*B*) T_{July} of Hudson (three-point moving average; solid line) and Moose lakes (three-point moving average; stippled line), and (*C*) tree-ring late-wood density in the central Brooks Range (50 y running mean; G. Jacoby, R. D'Arrigo, B. Buckley, IGBP PAGES/World Data Center for Paleoclimatology ITRDB AK032) with (*D*) T_{July} of Screaming Lynx Lake (three-point moving average).

growing-season temperature is available from the adjacent areas. The closest tree-ring data come from the Arrigetch area in the Brooks Range (data deposited in the IGBP PAGES/World Data Center for Paleoclimatology database, accession no. 3586), 409 km to the northwest of Screaming Lynx Lake. Despite their great distance, both temperature reconstructions reveal sustained cool summer temperatures until the first decade of the 20th century (Fig. 2 *C* and *D*). These and similar comparisons from other regions suggest that midge communities are sensitive to temperature fluctuations in the range of 0.5–2.0 °C (7, 12).

Patterns of Holocene Temperature Change. The Holocene T_{July} records from Hudson, Rainbow, and Screaming Lynx lakes have ranges of 11.2–12.9, 12.1–13.8, and 13.0–16.3 °C, respectively (Fig. 3 *B*–*D*). These records display some differences in their millennial-scale trends; for example, T_{July} decreased at Hudson and increased slightly at Rainbow between 10,000 and 6,000 cal B.P. Strikingly, however, none of the three records show persistently warmer-than-modern conditions during the first half of the Holocene, in contrast with precession-based predictions (Fig. 4*B*; see discussion below). To highlight the temporal patterns consistent among the sites, we derived a composite from these three records and a recently published T_{July} record from Moose Lake (7) for periods with at least three available records (past ~10,000 y) (Fig. 3*E*). This composite record shows cooler-than-average conditions for sustained periods during 10,000–5,500 cal B.P., interrupted by brief periods of near-modern temperature values. Peak values in the record occurred around 5,000 cal B.P., followed by a declining trend that culminates in a temperature minimum around 1,500 cal. B.P. These general patterns are robust to the exclusion of any individual site.

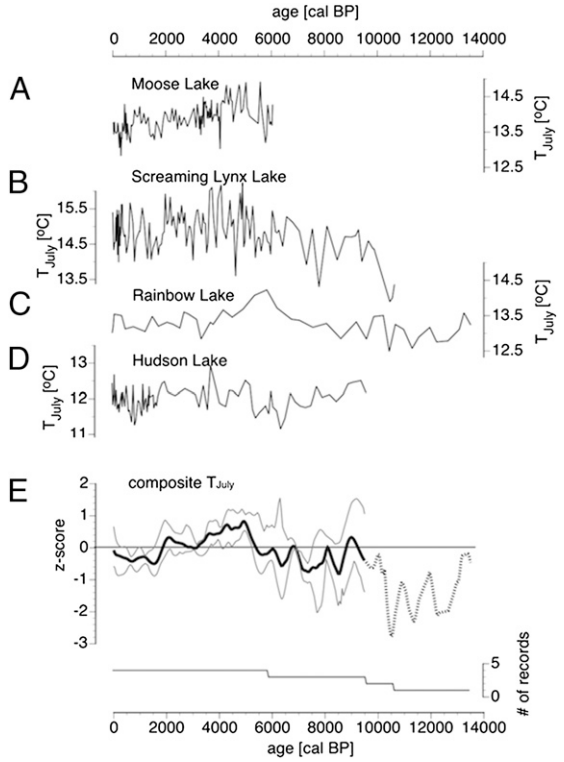

Fig. 3. Individual summer temperature records inferred from midge analysis of lake-sediment cores (*A*) Moose Lake (7); (*B*–*D*) data reported in this paper; and a composite (*E*) of the four records. Gray lines indicate 95% confidence intervals. Dotted line represents composite based on fewer than three sites.

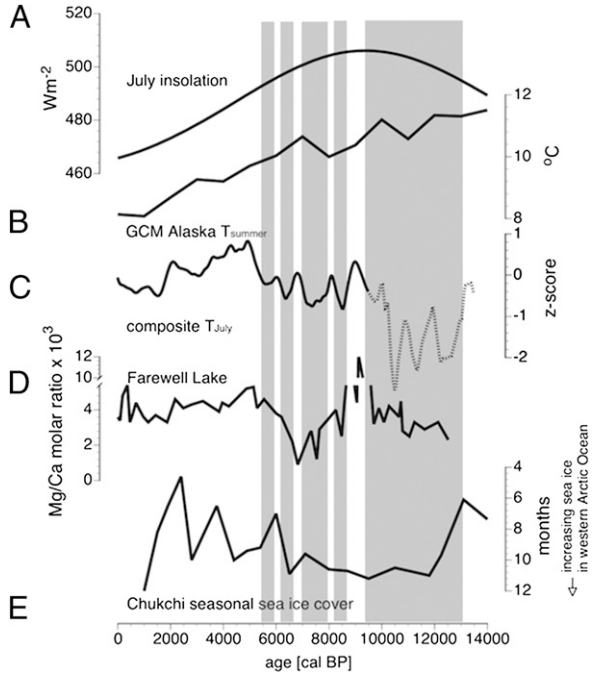

Fig. 4. Comparison of (*A*) July insolation at 65 °N latitude (2) and (*B*) GCM summer temperature over the Alaskan sector (mean over land surface) (16), with (*C*) a composite of four midge-based summer temperature records (Fig. 3*E*), (*D*) a qualitative, Mg/Ca summer temperature record from Farewell Lake, northwestern Alaska Range (5), and (*E*) dinoflagellate-inferred seasonal sea-ice cover in the eastern Chukchi Sea (8). Shaded areas correspond to early and middle Holocene periods with below-modern values in the composite temperature record.

T_{July} values from Hudson and Screaming Lynx lakes exhibit pronounced centennial-scale fluctuations (Fig. 3 *B* and *D*), some of which have magnitudes as large as the millennial-scale shifts in these records. A number of the temperature minima (e.g., 6,000–5,500, 3,500–3,300, 1,900–1,100, 500, and 250 cal B.P.) appear in other midge (7) and midge-independent climate records from Alaska (17), and have been attributed to climate responses to fluctuations in solar irradiance. However, several T_{July} minima appear to be temporally offset among individual records; these differences could represent true spatial variability, or merely age-depth model uncertainty. In the remainder of this paper, we focus on broad millennial trends, especially of the past ~10,000 y when three or more records are available.

Factors other than summer temperature, such as lake depth and terrestrial vegetation, also affect midge assemblages and thus could have confounded our T_{July} estimates (10). Passively loaded fossil samples in the canonical correspondence analysis (CCA) space of modern midge assemblages reveal variation along axis 1, which predominantly reflects T_{July} and dissolved organic carbon (DOC). Pronounced vegetational shifts occurred during the Holocene (e.g., ref. 18), which likely altered lake-water chemical composition, especially DOC concentration, and may have impacted midge assemblages. However, the millennial-scale T_{July} trends are unrelated to major vegetational transitions in the pollen records from the same areas (19, 20)

Midge assemblages from all three sites also vary along CCA axis 2, which is partially controlled by lake depth and lake surface area in modern samples (10). Sample scores on CCA axes 1 and 2 are negatively correlated at two of our sites (Screaming Lynx Lake: $r = -0.32$, $P < 0.01$, $n = 140$; Rainbow Lake: $r = -0.76$, $P < 0.01$, $n = 46$) (Fig. S4). This pattern could indicate an influence of lake-depth on T_{July} estimates, as low lake levels may

favor littoral midge taxa with relatively high temperature optima (11). However, paleolimnological studies in Alaska (5, 21, 22) have shown that the early Holocene was characterized by severe regional moisture deficits that reduced lake levels before ~8000 cal BP. To the extent that these low lake stands influenced midge communities, T_{July} values would be overestimated for the early Holocene, instead of underestimated. At Hudson Lake, CCA axes 1 and 2 are positively correlated ($r = 0.38$, $P < 0.01$, $n = 90$). We do not know of a biologically meaningful way in which lake-depth variations could have influenced T_{July} estimates in this manner.

Limited data from other sites are available for verification of our temperature reconstructions because most of the Holocene paleorecords from Alaska cannot be interpreted unambiguously in terms of summer temperature variations. A qualitative summer temperature record based on trace-element analysis from Farewell Lake, south-central Alaska, shows that the period of early-to-middle Holocene was generally colder than later except for a transient temperature maximum centered at ~9,000 cal B.P. (Fig. 4*D*) (5). Three other midge records are available from Alaska and adjacent Canada (5, 23). Estimates of T_{July} from these sites show either a flat Holocene temperature record or cooler-than-present conditions between 10,000 and 5,000 cal B.P. when using the same regional two-component weighted averaging partial least squares (WA-PLS2) inference model (10) that was applied to our sites, although at one of the sites estimated temperatures were higher between 18,000 and 11,000 cal B.P. than today. These records do not focus on the Holocene section, and many of the samples lack modern analogs, limiting their value for a detailed comparison with our data. Nonetheless, the results for the Holocene period are in general agreement with our findings, suggesting that the millennial-scale patterns consistent among them are robust and merit attention.

Nonlinear Response to Insolation Forcing: Potential Roles of Ocean–Atmosphere Feedbacks. July insolation at 65° N latitude reached peak values during the early Holocene and decreased gradually throughout the remainder of the Holocene (Fig. 4*A*). The Holocene T_{July} reconstruction from our midge assemblages is inconsistent with this broad pattern of insolation change, although the cooling trend from ~5,000 cal B.P. to present could reflect a direct response of T_{July} to orbital forcing. The absence of an orbital signal during the first half of our temperature time series is surprising, given that general circulation model (GCM) simulations have highlighted insolation as a key driver of Holocene millennial-scale temperature change in high-latitude regions, including Alaska (Fig. 4*B*) (16, 24). In addition, proxy-climate evidence for an early-to-middle Holocene thermal maximum has been reported from many areas of the Arctic (4); for example, treelines were up to 300 km farther north in central Siberia (25, 26). In Alaska, however, no evidence exists that the northern and western treelines have been beyond their modern limits during the Holocene, and tundra and forest tundra were common in many of today's forested areas during the early-to-middle Holocene. The relatively high abundance of *Populus* in many Alaskan pollen records has often been cited as evidence of early-Holocene thermal maximum between ~14,000–10,000 cal B.P. (4) (recent pollen records show that the *Populus* peaks occurred around 11500–10000 cal BP, on the basis of accelerator mass spectrometry dating of plant macrofossils). This interpretation is inconsistent with our T_{July} data from Rainbow Lake, the only one of our records that spans this period. *Populus* is found in the tundra north of spruce treelines today, and the *Populus*-dominated vegetation may have resulted from extensive soil disturbance on the early-postglacial landscapes, rather than directly from a thermal maximum (27).

The contrasting trajectories between our midge-inferred temperature record and Holocene summer insolation implicate major influences of factors other than direct precessional forcing on Alaskan summer temperature. Recent studies suggest that the mean atmospheric state of the early Holocene resembled the positive phase of the Arctic Oscillation (AO+) (8, 28–31). In addition to AO+ anomalies, coral records from the tropical Pacific indicate major changes in sea-surface temperature variability, which suggest a progressive increase in ENSO (El Niño-Southern Oscillation) frequency starting around 7,000 cal B.P. until modern periodicities were reached by ~5,000 cal B.P. (32). Furthermore, foraminifer trace-element records of tropical sea-surface temperature suggest predominantly La Niña-like conditions before ~4,000 cal B.P. (33). As at present, the prevalence of AO+ and La Niña-like conditions would have likely cooled land areas of Alaska during the early-to-middle Holocene.

Although temperature anomalies associated with the AO and ENSO are most pronounced in winter and spring, these atmospheric modes may have affected the Holocene trajectory of summer temperature via interseasonal anomalies of sea ice. Modern AO+ conditions result in a distinct dipole of sea-ice cover in the Arctic with increased summer sea-ice cover in the western Arctic Ocean (34). Evidence of sea-ice anomalies during the early-to-middle Holocene exists from Chukchi and Beaufort seas, where recent dinoflagellate and geochemical analyses revealed extensive summer sea ice and low sea-surface temperatures before ~6,000 cal B.P. (Fig. 4*E*) (8, 35). ENSO influences the sea-ice dipole between the eastern Bering Sea and the Sea of Okhotsk (36, 37), with increased sea-ice concentration in the Bering Sea during La Niña-like conditions (38). A diatom record from the Bering Sea confirms maximum sea-ice extent during the early Holocene and the persistence of greater-than-present ice cover through the middle Holocene (39), which are consistent with a response to a weakened Aleutian Low and prevailing northwesterly winds (39–42). Such sea-ice anomalies could have dampened spring- and summer-temperature effects of maximum insolation in Alaska. Furthermore, low spring temperatures associated with AO+ and La Niña-like conditions would have limited forest development in a vast area of Alaska before 6,000–5,000 cal B.P., resulting in elevated summer albedo and diminished summer temperature effects of high insolation (43). Today AO+ anomalies lead to enhanced effective moisture in Alaska, primarily by increasing winter precipitation. This pattern cannot be extrapolated to the early-to-middle Holocene, as low lake levels in Alaska suggest extreme aridity before ~8,000 cal B.P. (22). The maximal sea-ice extent was well beyond the modern range of variability in the Bering Sea before ~7,000 cal B.P. In combination with prevailing northwesterly winds, such sea-ice anomalies could have resulted in low winter precipitation (39).

Regardless of the precise mechanism, our data illustrate that Holocene summer-temperature variation in Alaska was not a linear function of solar forcing associated with precessional changes. This finding offers unique insights into the climatic drivers of Holocene ecosystem and landscape changes in northern high latitudes. For example, cool climatic conditions of the early-to-middle Holocene in Alaska could explain why treelines did not expand beyond their modern limits in that region but did so in many other regions of the Arctic (4, 24). These records also suggest that increasing effective moisture played an important role in the onset of neoglaciation in Alaska, as the late Holocene is not consistently colder than the period between 10,000 and 5,000 cal B.P.

Model experiments indicate that gradual changes in large-scale climatic drivers, such as insolation, can alter atmospheric circulation patterns and lead to nonlinear climatic responses at local to regional scales (44, 45). For example, coupled atmosphere–ocean GCMs show that millennial-scale shifts in the states of AO (25) and ENSO (46–48) may have resulted from gradual precessional changes in insolation, and they implicate that variability in these atmospheric modes played a key role in Holocene climate change. Given increasing concentrations of

atmospheric greenhouse gases and a possible return to predominantly positive-phase AO in the future (e.g., refs. 49–51), disentangling these feedbacks to radiative forcing and quantifying them in GCM simulations remain important challenges for projecting future change.

Materials and Methods

Sediment Collection and Correlation. Sediments were obtained from the deepest parts of Hudson, Screaming Lynx, and Rainbow lakes in the summers of 2005, 2007, and 2004, respectively. From each lake, two overlapping cores were taken with a modified Livingstone corer. A surface core with an intact mud–water interface was obtained with a piston-operated polycarbonate tube. The upper 10–20 cm of the surface cores were sectioned at 0.5-cm intervals in the field and the remainder of the cores sealed for transport. All cores from each lake were correlated using lithologic markers and magnetic susceptibility.

Chronologies. For chronological control, sediment samples from the top 20 cm were plated for ^{210}Pb activity (52, 53) and counted in an OctêtePlus alpha spectrometer at the University of Illinois. Ages were calculated using an "old-age corrected" constant-rate-of-supply model (54). For older sediments, a total of 44 terrestrial-macrofossil samples were selected for ^{14}C analysis (Dataset S1, Dataset S2, and Dataset S3 for Hudson, Screaming Lynx, and Rainbow lakes, respectively). These samples were pretreated (55) in a laminar flowhood and analyzed at the Center for Accelerator Mass Spectrometry, Lawrence Livermore National Laboratory. ^{14}C ages were calibrated to years before A.D. 1950 (cal B.P.) in CALIB v.5.01 (56, 57). An age model was calculated for each lake from the ^{210}Pb and ^{14}C ages using a weighted cubic smoothing spline function (58).

Midge Assemblage Analysis. Wet-sediment samples (2–3 cm^3 each) were treated following standard procedure (9). Samples were sieved with a 90-μm mesh. All head capsules of chironomids and ceratopogonids as well as *Chaoborus* mandibles in the residue were isolated, dried onto standard microscope slides, mounted using Entellan, and identified (59–61). Taxonomic resolution was harmonized with the applied transfer function (see below) (10). The midge assemblage data are available as supporting datasets (Dataset S1, Dataset S2, and Dataset S3 for Hudson, Screaming Lynx, and Rainbow lakes, respectively).

Temperature Inferences. We estimated T_{July} from midge assemblages using a WA-PLS2 model with a reported error envelope of 1.46 °C (10). The model training set includes surface-sediment samples from sites spanning Alaska and neighboring regions (British Columbia, Yukon Territory, Northwest Territories). Temperature estimates were obtained only if a sample contained >50 midge head capsules (62). Midge assemblages for each fossil sample were passively loaded in a CCA of the training set to determine the dominant environmental drivers of variation. The youngest samples from Hudson, Rainbow, and Screaming Lynx were compared with the mean July temperatures of equivalent years corrected for a dry adiabatic rate of 9.8 °C/km from weather stations at Gulkana, Kenai, and Fort Yukon, respectively, to assess the fidelity of T_{July} inferences at each site.

Regional Temperature Composite. To facilitate comparison of Holocene temperature trajectories with other paleoclimate records, we created a composite of our midge T_{July} data and an additional Alaskan summer temperature record with strong chronological control (Fig. 1) (7). The individual records were converted into *z*-scores to standardize the mean and variance. The composite T_{July} record was then computed as a locally weighted regression (63) through the full set of transformed data using a 2,000-y moving window. Confidence envelopes were estimated by bootstrapping (n = 1,000) wherever three or more records contribute to the composite. Bootstrap samples consisted of individual lake records, drawn with replacement (n = 4). Error envelopes reflect variability among records.

ACKNOWLEDGMENTS. We thank J. Ko and S. Harding Forrester for the separation and mounting of midge head capsules; C. Barrett, E. Berg, A. Henderson, and P. Higuera for assistance in the field; and J. Beer, W. Tinner, and J. Walsh for insightful discussions. Comments from C. Barrett, C. Cáceres, M. Chipman, M. Clegg, O. Heiri, H. Lauren, T. Johnson, M. Urban, and two anonymous reviewers greatly improved the manuscript. Funding for this research was provided by National Science Foundation (NSF) Grants ARC 0455102 and ARC 0612366 (to F.S.H.). B.F.C. was supported by a NSF Doctoral Dissertation Improvement Grant and a Doctoral Dissertation Completion Fellowship from the Graduate College of the University of Illinois.

1. Thompson DWJ, Wallace JM (1998) The Arctic Oscillation signature in the wintertime geopotential height and temperature fields. *Geophys Res Lett* 25:1297–1300.
2. Laskar J, et al. (2004) A long-term numerical solution for the insolation quantities of the Earth. *Astron Astrophys* 428:261–285.
3. CAPE Project Members (2001) Holocene paleoclimate data from the Arctic: Testing models of global climate change. *Quat Sci Rev* 20:1275–1287.
4. Kaufman DD, et al. (2004) Holocene thermal maximum in the western Arctic (0-180° W). *Quat Sci Rev* 23:529–560.
5. Hu FS, Ito E, Brubaker LB, Anderson PM (1998) Ostracode geochemical record of Holocene climatic change and implications for vegetational response in the northwestern Alaska Range. *Quat Res* 49:86–95.
6. Kurek J, Cwynar LC, Ager TA, Abbott MA, Edwards ME (2009) Late Quaternary paleoclimate of western Alaska inferred from fossil chironomids and its relation to vegetation histories. *Quat Sci Rev* 28:799–811.
7. Clegg BF, et al. (2010) Six millennia of summer temperature variation based on midge analysis of lake sediments from Alaska. *Quat Sci Rev* 29:3308–3316.
8. de Vernal A, Hillaire-Marcel C, Darby DA (2005) Variability of sea ice cover in the Chukchi Sea (western Arctic Ocean) during the Holocene. *Paleoceanography* 20: PA4018.
9. Walker IR, Smol JP, Engstrom DR, Birks HJB (1991) An assessment of Chironomidae as quantitative indicators of past climatic change. *Can J Fish Aquat Sci* 48:975–987.
10. Barley EM, et al. (2006) A northwest North American training set: Distribution of freshwater midges in relation to air temperature and lake depth. *J Paleolimnol* 36: 295–314.
11. Velle G, Brodersen KP, Birks HJB, Willassen E (2010) Midges as quantitative temperature indicator species: Lessons for palaeoecology. *Holocene* 20:989–1002.
12. Larocque I, Hall RI (2003) Chironomids as quantitative indicators of mean July air temperature: Validation by comparison with century-long meteorological records from northern Sweden. *J Paleolimnol* 29:475–493.
13. Heiri O, Lotter AF, Hausmann S, Kienast F (2003) A chironomid-based Holocene summer air temperature reconstruction from the Swiss Alps. *Holocene* 13:477–484.
14. Davi NK, Jacoby GC, Wiles GC (2003) Boreal temperature variability inferred from maximum latewood density and tree-ring width data, Wrangell Mountain region, Alaska. *Quat Res* 60:252–262.
15. Wiles GC, D'Arrigo RD, Villalba R, Calkin PE, Barclay DJ (2004) Century-scale solar variability and Alaskan temperature change over the past millennium. *Geophys Res Lett* 31:L15203.
16. Singarayer JS, Valdes PJ (2010) High-latitude climate sensitivity to ice-sheet forcing over the last 120 kyr. *Quat Sci Rev* 29:43–55.
17. Hu FS, et al. (2003) Cyclic variation and solar forcing of Holocene climate in the Alaskan subarctic. *Science* 301:1890–1893.
18. Brubaker LB, Anderson PM, Hu FS (2001) Vegetation ecotone dynamics in southwest Alaska during the late Quaternary. *Quat Sci Rev* 20:175–188.
19. Tinner W, et al. (2006) Postglacial vegetational and fire history: Pollen, plant macrofossil and charcoal records from two Alaskan lakes. *Veget Hist Archaeobot* 15: 279–293.
20. Anderson PM, Brubaker LB (1994) Holocene vegetation and climate histories of northcentral Alaska: A mapped summary of late-Quaternary pollen data. *Quat Sci Rev* 13:71–92.
21. Bigelow NH (1997) Late-Quaternary vegetation and lake-level changes in central Alaska. PhD dissertation (University of Alaska, Fairbanks).
22. Abbott MB, Finney BP, Edwards ME, Kelts KR (2000) Lake-level reconstructions and paleohydrology of Birch Lake, central Alaska, based on seismic reflection profiles and core transects. *Quat Res* 53:154–166.
23. Kurek J, Cwynar LC, Vermaire JC (2009) A late Quaternary paleotemperature record from Hanging Lake, northern Yukon Territory, eastern Beringia. *Quat Res* 72: 246–257.
24. Renssen H, Seppä H, Heiri O, Goosse H, Fichefet T (2009) The spatial and temporal complexity of the Holocene thermal maximum. *Nat Geosci* 2:411–414.
25. Khotinskiy NA (1984) *Late Quaternary Environments of the Soviet Union*, eds Wright HE, Jr., Barnosky CW (Univ of Minnesota Press, Minnesota), pp 179–200.
26. MacDonald GM, et al. (2000) Holocene treeline history and climate change across northern Eurasia. *Quat Res* 53:302–311.
27. Hu FS, Brubaker LB, Anderson PM (1993) A 12,000 year record of vegetation change and soil development from Wien Lake, central; Alaska. *Can J Bot* 71:1133–1142.
28. Rimbu N, Lohmann G, Kim J-H, Arz W, Schneider R (2003) Arctic/North Atlantic Oscillation signature in Holocene sea surface temperature trends as obtained from alkenone data. *Geophys Res Lett* 30:1280.
29. Andersen C, Koç N, Jennings A, Andrews JT (2004) Nonuniform response of the major surface currents in the Nordic Seas to insolation forcing: Implications for the Holocene climate variability. *Paleoceanography* 19:PA2003.
30. de Vernal A, Hillaire-Marcel C (2006) Provincialism in trends and high frequency changes in the northwest North Atlantic during the Holocene. *Global Planet Change* 54:263–290.
31. Bendle JAP, Rosell-Melé A (2007) High-resolution alkenone sea surface temperature variability on the North Icelandic shelf: Implications for Nordic Seas paleoclimatic development during the Holocene. *Holocene* 17:9–24.
32. Rodbell DT, et al. (1999) An approximately 15,000-year record of El Nino-driven alluviation in southwestern ecuador. *Science* 283:516–520.

33. Marchitto TM, Muscheler R, Ortiz JD, Carriquiry JD, van Geen A (2010) Dynamical response of the tropical Pacific Ocean to solar forcing during the early Holocene. *Science* 330:1378–1381.
34. Rigor IG, Wallace JM, Colony RL (2002) Response of sea ice to the Arctic Oscillation. *J Clim* 15:2648–2663.
35. McKay JL, et al. (2008) Holocene fluctuations in Arctic sea-ice cover: Dinocyst-based reconstructions for the eastern Chukchi Sea. *Can J Earth Sci* 45:1377–1397.
36. Cavalieri DJ, Parkinson CL (1987) On the relationship between atmospheric circulation and the fluctuations in the sea ice extents of the Bering and Okhotsk Seas. *J Geophys Res* 92:7141–7162.
37. Alexander MA, Tomas R, Deser C, Lawrence DM (2010) The atmospheric response to projected terrestrial snow changes in the late twenty-first century. *J Clim* 23: 6430–6437.
38. Niebauer HJ (1988) Effects of El Niño–Southern Oscillation and North Pacific weather patterns on interannual variability in the subarctic Bering Sea. *J Geophys Res* 93: 5051–5068.
39. Katsuki K, et al. (2009) Land-sea linkage of Holocene paleoclimate on the Southern Bering Continental Shelf. *Holocene* 19:747–756.
40. Honda M, Nakamura H, Ukita J, Kousaka I, Takeuchi K (2001) Interannual seesaw between the Aleutian and Icelandic Lows. Part I: Seasonal dependence and life cycle. *J Clim* 14:1029–1042.
41. Sasaki YN, Minobe S (2005) Seasonally dependent interannual variability of sea ice in the Bering Sea and its relation to atmospheric fluctuations. *J Geophys Res* 110: C05011.
42. Pozo-Vázques D, Esteban-Parra MJ, Rodrigo FS, Castro-Díez T (2001) The association between ENSO and winter atmospheric circulation and temperature in the North Atlantic region. *J Clim* 14:3408–3420.
43. Foley JA, Kutzbach JE, Coe MT, Levis S (1994) Feedbacks between climate and boreal forests during the Holocene epoch. *Nature* 371:52–54.
44. DeMenocal P, et al. (2000) Abrupt onset and termination of the African humid period: Rapid climate responses to gradual insolation forcing. *Quat Sci Rev* 19:347–361.
45. Hodell DA, et al. (2001) Abrupt cooling of Antarctic surface waters and sea ice expansion in the South Atlantic sector of the Southern Ocean at 5000 cal yr BP. *Quat Res* 56:191–198.
46. Bush ABG (1999) Assessing the impact of Mid-Holocene insolation on the atmosphere-ocean system. *Geophys Res Lett* 26:99–102.
47. Clement AC, Seager R, Cane MA (2000) Suppression of El Niño during the mid-Holocene by changes in the Earth's orbit. *Paleoceanography* 15:731–737.
48. Liu Z, Kutzbach J, Wu L (2000) Modeling climate shift of El Niño variability in the Holocene. *Geophys Res Lett* 27:2265–2268.
49. Shindell DT, Miller RL, Schmidt GA, Pandolfo L (1999) Simulation of recent northern winter climate trends by greenhouse-gas forcing. *Nature* 399:452–455.
50. Rind D, Perlwitz J, Lonergan P, Lerner J (2005) AO/NAO response to climate change: 2. Relative importance of low- and high-latitude temperature changes. *J Geophys Res* 110:D12.
51. Stephenson DB, Pavan V, Collins M (2006) North Atlantic Oscillation response to transient greenhouse gas forcing and the impact on European winter climate: A CMIP2 multi-model assessment. *Clim Dyn* 27:401–420.
52. Eakins JD, Morrison RT (1978) A new procedure for the determination of lead-210 in lake and marine sediments. *Int J Appl Radiat Isot* 29:531–536.
53. Benoit G, Hemond HF (1987) A biogeochemical mass balance of ^{210}Po and ^{210}Pb in an oligotrophic lake with seasonally anoxic hypolimnion. *Geochim Cosmochim Acta* 51: 1445–1456.
54. Binford MW (1990) Calculation and uncertainty analysis of ^{210}Pb dates for PIRLA project lake sediment cores. *J Paleolimnol* 3:252–267.
55. Oswald WW, et al. (2005) Effects of sample mass and macrofossil type on radiocarbon dating of arctic and boreal lake sediments. *Holocene* 15:758–767.
56. Stuiver M, Reimer PJ (1993) Extended ^{14}C data base and revised CALIB 3.0 ^{14}C age calibration program. *Radiocarbon* 35:215–230.
57. Reimer PJ, et al. (2004) Intcal04 terrestrial radiocarbon age calibration, 0-26 cal kyr B.P. *Radiocarbon* 46:1029–1058.
58. Higuera PE, Brubaker LB, Anderson PM, Hu FS, Brown TA (2009) Vegetation mediated the impacts of postglacial climatic change on fire regimes in the south-central Brooks Range. *Ecol Monogr* 79:201–219.
59. Wiederholm T (1983) Chironomidae of the Holarctic Region. keys and diagnoses. Part 1. Larvae. *Entomol Scand* (Suppl 19):1–457.
60. Oliver DR, Roussel ME (1983) *The Insects and Arachnids of Canada, Part 11: The Genera of Larval Midges of Canada, Diptera: Chironomidae* (Research Branch, Agriculture Canada, Ottawa), pp 1–263.
61. Brooks SJ, Langdon PG, Heiri O (2007) The identification and use of palaearctic Chironomidae larvae in Palaeoecology. *Quaternary Research Association. Technical Guide* 10:1–276.
62. Heiri O, Lotter AF (2001) Effect of low count sums on quantitative environmental reconstructions: An example using subfossil chironomids. *J Paleolimnol* 26:343–350.
63. Cleveland WS (1979) Robust locally weighted regression and smoothing scatterplots. *J Am Stat Assoc* 74:829–836.